



ELSEVIER

Available online at www.sciencedirect.com

**ScienceDirect**

www.elsevier.com/locate/jmbbm

**Research Paper****Micro- and nano-mechanics of osteoarthritic cartilage: The effects of tonicity and disease severity**

P.R. Moshtagh<sup>a,b,\*</sup>, B. Pouran<sup>a,b</sup>, J. van Tiel<sup>d</sup>, J. Rauker<sup>a</sup>, M.R. Zuiddam<sup>e</sup>, V. Arbabi<sup>a</sup>, N.M. Korthagen<sup>b,f</sup>, H. Weinans<sup>a,b,c</sup>, A.A. Zadpoor<sup>a</sup>

<sup>a</sup>Faculty of Mechanical, Maritime, and Materials Engineering, Delft University of Technology (TU Delft), Mekelweg 2, 2628 CD, Delft, The Netherlands

<sup>b</sup>Department of Orthopaedics, University Medical Center Utrecht, Q.03.2.103-1, Heidelberglaan 100, 3584 CX, Utrecht, The Netherlands

<sup>c</sup>Department of Rheumatology, University Medical Center Utrecht, Utrecht, The Netherlands

<sup>d</sup>Department of Orthopaedics and Radiology, Erasmus Medical Centre, Rotterdam, The Netherlands

<sup>e</sup>Kavli Institute of Nanoscience, Delft University of Technology, Lorentzweg 1, 2628 CJ, Delft, The Netherlands

<sup>f</sup>Department of Equine Sciences, Faculty of Veterinary Medicine, Utrecht University, Utrecht, The Netherlands

**ARTICLE INFO****Article history:**

Received 17 November 2015

Received in revised form

23 February 2016

Accepted 9 March 2016

Available online 24 March 2016

**Keywords:**

Articular cartilage

Biophysics

Osmolality

EPIC- $\mu$ CT

Nano-stiffness

Micro-stiffness

**ABSTRACT**

The present study aims to discover the contribution of glycosaminoglycans (GAGs) and collagen fibers to the mechanical properties of the osteoarthritic (OA) cartilage tissue. We used nanoindentation experiments to understand the mechanical behavior of mild and severe osteoarthritic cartilage at micro- and nano-scale at different swelling conditions. Contrast enhanced micro-computed tomography (EPIC- $\mu$ CT) was used to confirm that mild OA specimens had significantly higher GAGs content compared to severe OA specimens. In micro-scale, the semi-equilibrium modulus of mild OA specimens significantly dropped after immersion in a hypertonic solution and at nano-scale, the histograms of the measured elastic modulus revealed three to four components. Comparing the peaks with those observed for healthy cartilage in a previous study indicated that the first and third peaks represent the mechanical properties of GAGs and the collagen network. The third peak shows considerably stiffer elastic modulus for mild OA samples as compared to the severe OA samples in isotonic conditions. Furthermore, this peak clearly dropped when the tonicity increased, indicating the loss of collagen (pre-) stress in the shrunk specimen. Our observations support the association of the third peak with the collagen network. However, our results did not provide any direct evidence to support the association of the first peak with GAGs. For severe OA specimens, the peak associated with the collagen network did

\*Corresponding author at: Department of Orthopaedics, University Medical Center Utrecht, Uppsalaalaan 8, 3584 CT Utrecht, Netherlands. Tel.: +31 623721926.

E-mail addresses: P.Rahnamaymoshtagh@umcutrecht.nl (P.R. Moshtagh), B.Pouran@umcutrecht.nl (B. Pouran), J.Vantiel@erasmusmc.nl (J. van Tiel), Jrauker@m3dd.com (J. Rauker), M.R.Zuiddam@tudelft.nl (M.R. Zuiddam), V.arbabi-21@tudelft.nl (V. Arbabi), N.M.Korthagen@uu.nl (N.M. Korthagen), H.H.Weinans@umcutrecht.nl (H. Weinans), A.A.Zadpoor@tudelft.nl (A.A. Zadpoor).

not drop when the tonicity increased, indicating a change in the response of OA cartilage to hypertonicity, likely collagen damage, as the disease progresses to its latest stages.

© 2016 Elsevier Ltd. All rights reserved.

## 1. Introduction

Articular cartilage, with its heterogeneous hydrated mesh-work and interpenetrated polymeric components exhibits a complex biomechanical behavior (Julkunen, 2008; Nimer et al., 2003; Stolz et al., 2009). Particularly, negatively charged Glycosaminoglycan chains (GAGs) interact with the positive ions from the environment and create a high tonicity that causes the cartilage to swell. The subsequent swelling pressure is then counteracted by collagen (type 2) fibers. Any degenerative changes in the articular cartilage macromolecules disrupt the "structure–function" of its network and trigger changes in the functionality of these polymeric constituents (Loparic et al., 2010). Osteoarthritis (OA) is a degenerative joint disease that is characterized by the loss of proteoglycans (PGs) and hence GAG content via enzymes (mainly matrix metalloproteases and aggrecanases) as well as failure of the collagen network and subsequently loss of cartilage stiffness (Ghosh and Smith, 2002; Hedbom, 2002; Ishiguro and Poole, 2002).

Mechanical properties at the molecular to tissue levels can be obtained by indentation machines, that can perform indentations at the homogenized tissue level (often referred to as microindenter or nanoindenter) and at the molecular level (using indentation type Atomic Force Microscopy, IT-AFM). For instance, (Miller and Morgan, 2010) have determined the macro and micro-scale mechanical features and the biphasic properties of the femoropatellar portion of bovine cartilage. (Li et al., 2011) have measured the modulus of porcine cartilage and polyacrylamide gel by applying stress relaxation analysis using nanoindentation and found the possibility to tailor the mechanical properties of hydrogel materials for cartilage tissue engineering purposes. Moreover, Stolz and colleagues have used IT-AFM in a number of studies to characterize the mechanical properties of the cartilage and found it an appropriate method to characterize early OA (Loparic et al., 2010; Stolz et al., 2004, 2009). Similarly, Grodzinsky and colleagues have assessed the time-dependent nano-stiffness of articular cartilage using IT-AFM to quantify its frequency and time-dependent behavior (Han et al., 2011; Nia et al., 2011, 2013).

The aim of the current study is to understand the response of OA cartilage to changes in ionic strength (tonicity) and correlate it with (i) the mechanical properties of cartilage measured at the micro- and nano-scale measured using indentation experiments and (ii) the severity of the disease. The response of OA cartilage to changes in tonicity could indirectly give us information about the relationship between the structure and properties of cartilage, because the porous hydrated matrix with its negatively charged GAGs and fibrillar collagen macromolecules is responsible for cartilage's biomechanical behavior. Under different external tonicities,

cartilage has different swelling behaviors as a consequence of GAGs and the resultant collagen fiber pretension. Thus, different mechanical characteristics for its individual components would be expected after dehydration as a consequence of tonicity changes, and nanoindentation enables us to entangle the properties of collagens from those of GAGs. Moreover, the progression of the disease to mild OA and ultimately severe OA may disrupt the mechanical interaction between collagen and GAGs, which could be elucidated from the micro- and nano-scale indentations.

## 2. Materials and methods

### 2.1. Specimen preparation

Human osteoarthritic (OA) articular cartilage specimens (harvested from the weight bearing part of femoral condyles and the tibial plateaus and parallel to the surface of the cartilage with intact surface) with different levels of disease severity (mild and severe based on the Kellgren and Lawrence classification) were harvested during total knee replacement surgeries (Fig. 1). The samples were subsequently buffered in Phosphate Buffer Sulfate (PBS, Gibco, UK) 1% and stored at  $-20^{\circ}\text{C}$  (Athanasou et al., 1991; Wilusz et al., 2013). Before the indentation experiments, the cartilage samples were attached to a substrate using water-resistant epoxy-based glue and were covered by a PBS solution. We used two different PBS solutions: normal PBS as an isotonic solution (containing 155 mM NaCl) and a hypertonic PBS solution (containing 2 M NaCl), in both cases combined with a protease inhibitor cocktail (complete, Roche, Mannheim, Germany). We performed the mechanical tests such as creep and dynamic indentation using nano-indenter and IT-AFM on 5 mild OA samples and 5 severe OA samples.

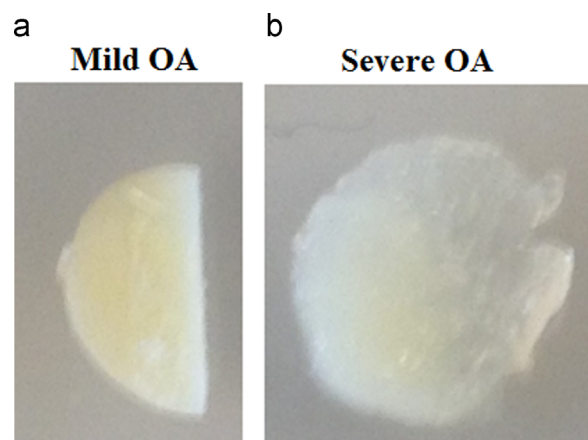
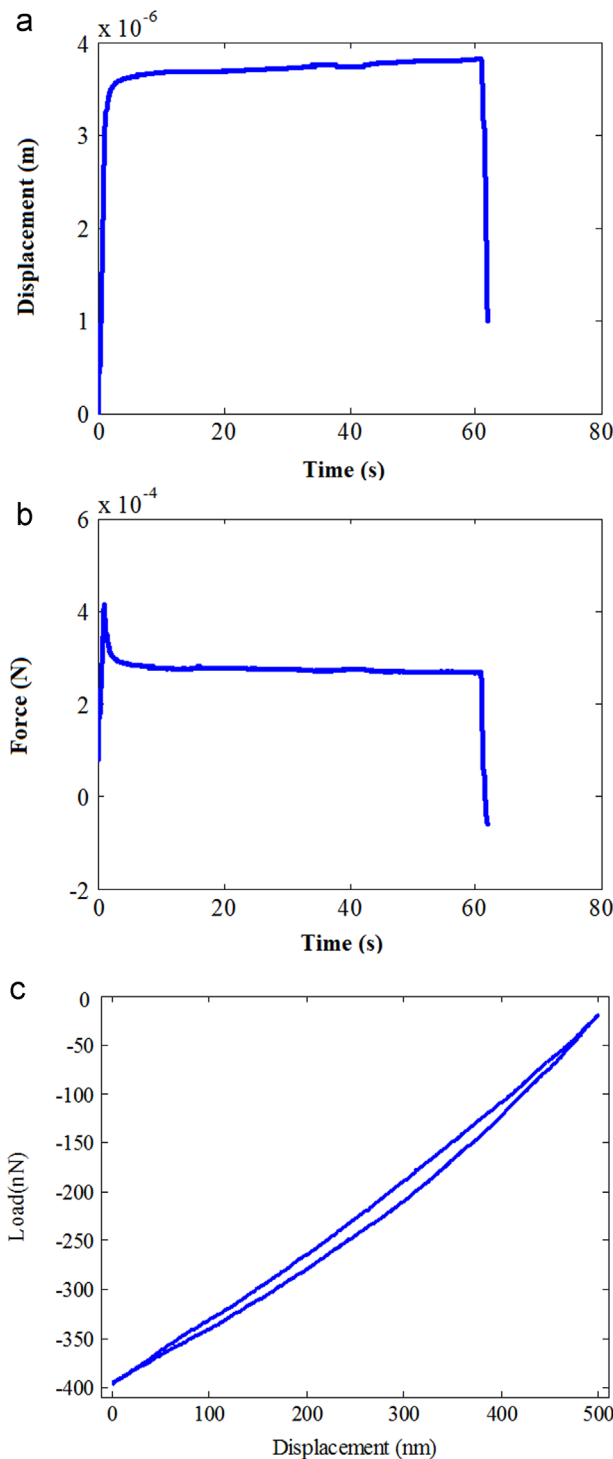


Fig. 1 – (a) Mild and (b) severe OA samples.



**Fig. 2 – Displacement-time (a) and force-time, (b) graphs of micro-scale creep data by nanoindenter, (c) load-displacement curve by IT-AFM.**

## 2.2. Indentation experiments

### 2.2.1. Micro-scale

For the micro-scale measurements, a nanoindenter machine (Hysitron, USA) was used to obtain indentation-based creep curves on mildly OA cartilage specimens only (Fig. 1a). The cartilage network in the severely OA specimens was highly

disrupted, rendering consistent micro-scale indentations infeasible. The mild and severe OA specimens differed in their macroscopic damage in terms of the amount of cartilage fibrillation and color change. They also had different shapes and thicknesses (Figs. 6a and 7). In order to prevent overstressing, we selected a diamond conospherical fluid-type probe with a tip radius of 44.42  $\mu\text{m}$ . Before starting the experiments, the specimens were thawed and kept in isotonic PBS solution for 1 h. Thereafter, a series of indentation tests were performed. The indentation is intended as a creep experiment that uses motor-controlled displacements with continuously measured loading that is corrected in the feedback system to ensure that a constant load of  $3 \times 10^{-4}$  N is applied throughout the indentation experiment. The feedback correction results in a small overshoot in the first second that is adjusted to  $3 \times 10^{-4}$  N thereafter. The maximum load was then maintained for 60 s and corresponded to a total displacement of 3000–4900 nm (Fig. 2a).

The medium was then replaced by the hypertonic solution and several creep indentation experiments were performed at 20, 40, 60, and 120 min after immersion of the sample in the hypertonic solution. All above-mentioned tests were performed on two or more different locations (points) on each cartilage samples and for each time point. The creep indentation tests were repeated three times per each location with 120 s recovery times between the repetitions.

To obtain the semi-equilibrium modulus from the creep test, we applied the method that is developed by Oyen (2013) using Prony series to fit a curve to the creep data in order to calculate the long term shear modulus of the material sample in the first step (Fig. 2b). Then, by assuming a Poisson's ratio of 0.5 for the cartilage sample (considering the incompressibility assumption (jin and Lewis, 2004; Loparic et al., 2010; Richard et al., 2013; Stolz et al., 2004), Young's modulus could be calculated. The analytical relationships were fitted to the experimental data using the following equations (Moyer et al., 2012; Oyen, 2009, 2013)

$$h^{\frac{1}{2}}(t) = A_0 - \sum A_i \exp(-t/\tau_i) \quad (1)$$

$$C_0 = \frac{8A_0\sqrt{R}}{3P_{\max}} \quad (2)$$

$$C_i = \frac{8A_i\sqrt{R}}{(RCF_i)3P_{\max}} \quad (3)$$

$$(RCF_i) = \frac{\tau_i}{\tau_R} [\exp(\tau_R/\tau_i) - 1] \quad (4)$$

$$G = \frac{1}{2 \times (C_0 - \sum C_k)} \quad (5)$$

$$E = G \times 2 \times (1 + \nu) \quad (6)$$

where  $A_0, \dots, A_k$  are the creep parameters,  $h$  is the indentation depth,  $P_{\max}$  is the maximum applied force,  $\nu$  is Poisson's ratio of the soft specimen, and  $R$  is the radius of the spherical indenter. Considering a step-loading profile for the creep test,  $\tau_R$  is the total ramp time and  $RCF_i$  is the ramp correction factor for creep.

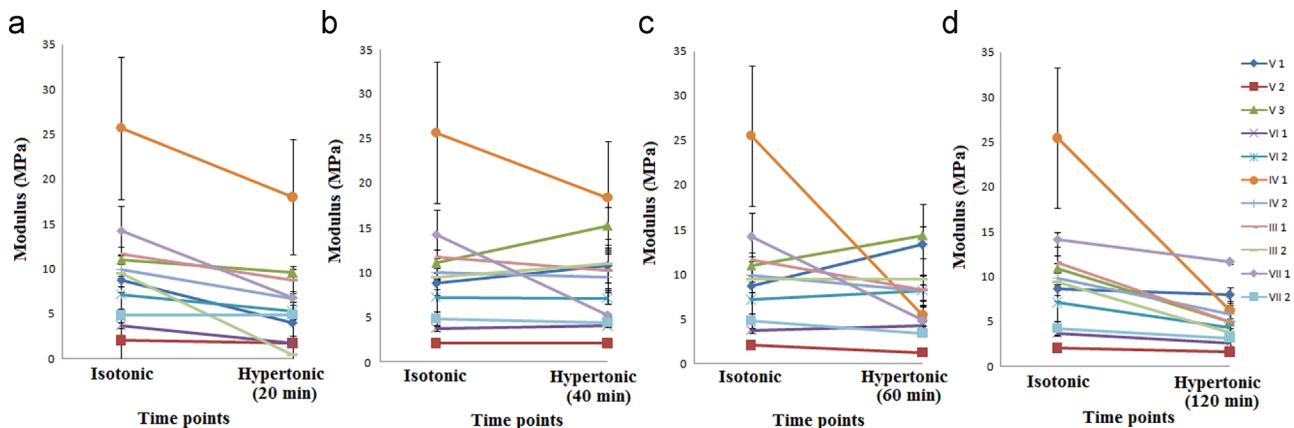


**Fig. 3 – Micro-stiffness of mild OA cartilage samples at two different ionic strengths of the PBS solution at different time points: first isotonic PBS then after 20 min incubation in hypertonic PBS (a), after 40 min (b), after 60 min (c), after 120 min (d).**

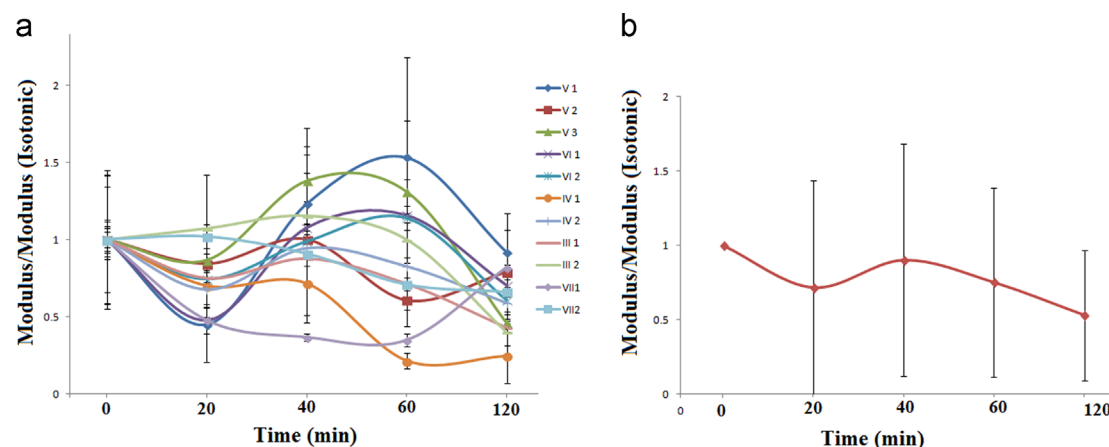


**Fig. 4 – Normalized modulus number of each time point in hypertonic PBS scaled for the modulus in normal PBS (a). Normalized modulus number of each time point for all samples per mean modulus in normal PBS (b).**

### 2.2.2. Nano-scale

For the nano-scale measurements, an atomic force microscope equipped with a nanoscope controller (Bruker, Dimension V, Japan) and a standard fluid cell (Bruker) with a nanometer sized pyramidal tip (nominal radius: 15 nm and cantilever spring constant: 0.06 N/m) (Nano and More, Germany) was used to obtain indentation-based force-displacement curves on both the severe and mild human OA cartilage samples (Fig. 7). Before starting the experiments, the thermal fluctuations technique was employed to calculate the exact values of the cantilever spring constant. Afterwards, the load-displacement curves were acquired at a frequency of 3 Hz corresponding to an indentation rate of 3  $\mu\text{m}/\text{s}$  (Stolz, 2009) (Fig. 2c). First, the experiment was done on the surface of the sample within normal PBS solution (isotonic condition) during 2 h and then the medium was changed to hypertonic PBS (hypertonic condition) and the same procedure was followed on the same specimen. The maximum indentation depth was adjusted around 500 nm. Each force-displacement curve consisted of 1024 data points. In total, around 3000 indentation curves were obtained for 5 different specimens. The nanoscope (Bruker, version 1.4) analysis software was

used to analyse the obtained force-displacement curves and to calculate Young's modulus based on the Hertz's contact theory.

In order to calculate the dynamic elastic modulus (Stolz et al., 2004, 2009) at each point we used Sneddon's theory that relates force ( $P$ ) to displacement ( $h$ ) through the following relationship (Oyen and Cook, 2009; Xie et al., 2010)

$$P = \frac{\pi \tan \varphi}{2\gamma^2} \frac{E}{1-\nu^2} h^2 \quad (7)$$

where  $\varphi$  is the half angle of the cone,  $\gamma=\pi/2$ ,  $\nu$  is Poisson's ratio.

The histogram of the measured elastic moduli was first established and then converted to a probability distribution function by dividing the corresponding frequency of every histogram bin by the total number of measurements. All indentations on the five separate specimens were lumped in one probability density function (frequency histogram) and the data from all 5 samples were pooled together. To objectively quantify the mean and standard deviation of the different constituents represented in the probability density function, a finite Gaussian mixture model (Zadpoor, 2015) was fitted to the measured probability density function. In

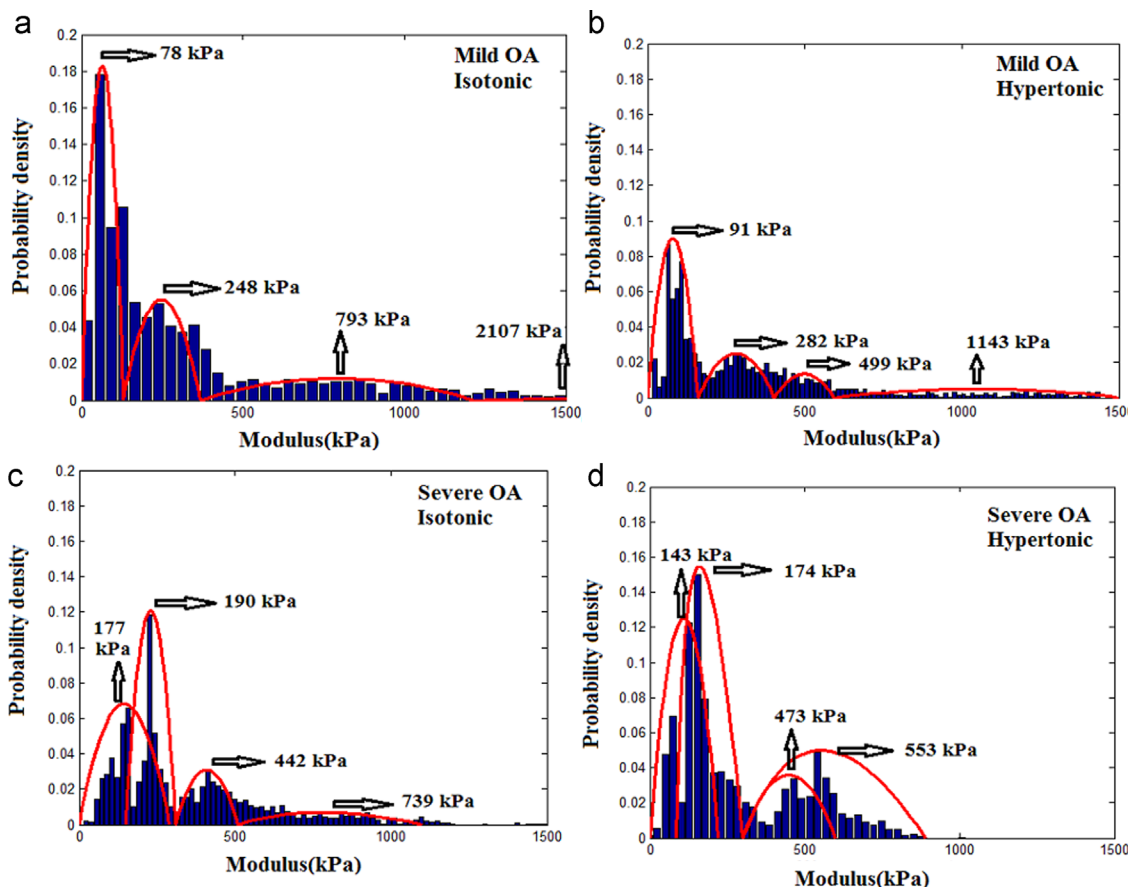


**Fig. 5 – The probability density distribution of the measured elastic modulus values at the nano-scale and the corresponding 4-components Gaussian finite mixture model. The data is presented for mild OA cartilage samples in isotonic conditions (a), mild OA samples in hypertonic conditions (b), severe OA cartilage in isotonic conditions (c), and severe OA cartilage in hypertonic conditions (d).**

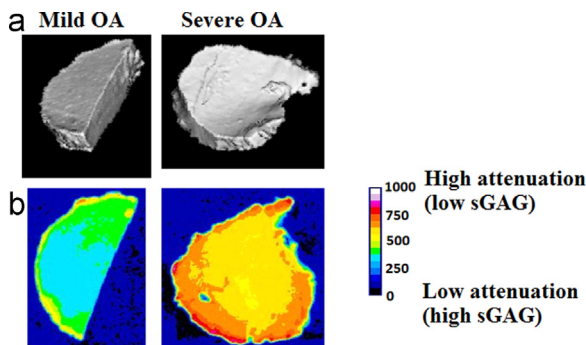


**Fig. 6 – Micro-CT image of two specimens from mild and severe OA groups (a), EPIC- $\mu$ CT images of two representative specimens from mild and severe OA groups (b). The distribution of ioxaglate through the x-ray attenuation values (arbitrary unit) is represented where extremely high ioxaglate concentration is shown with bright color and extremely low ioxaglate concentration is shown with blue. For every group, the representative specimen is the one that has the closest average gray value to the average gray value of its group. (For interpretation of the references to color in this figure legend, the reader is referred to the web version of this article.)**

the finite Gaussian mixture models, it is assumed that the probability distribution function,  $f(x)$ , measured for a multi-constituent material is the weighted sum of the Gaussian probability distributions,  $N(\mu_i, \sigma_i)$ , measured for every constituent  $i$ :

$$f(x) = \sum_{i=1}^m w_i N(\mu_i, \sigma_i) \quad (8)$$

where  $\mu_i$ ,  $\sigma_i$ , and  $w_i$  are respectively mean, standard deviation, and weighting factor of every constituent. The number of components,  $m$ , was increased to obtain the minimum number of components that could capture all the peaks present in the measured probability density distributions. An iterative algorithm based on the long-likelihood criterion was used for fitting the mixture of the Gaussian distributions to the experimental data. The iterative algorithm was stopped when the solution converged within a tolerance of 1E-6 (Zadpoor, 2015).

### 2.3. Contrast enhanced micro-CT (EPIC- $\mu$ CT)

Prior to saturation with contrast agent, samples underwent micro-CT scan (Quantum FX, Perkin Elmer, USA) under 90 kV tube voltage, 180  $\mu$ A tube current, 40  $\mu$ m voxel size and 2 min

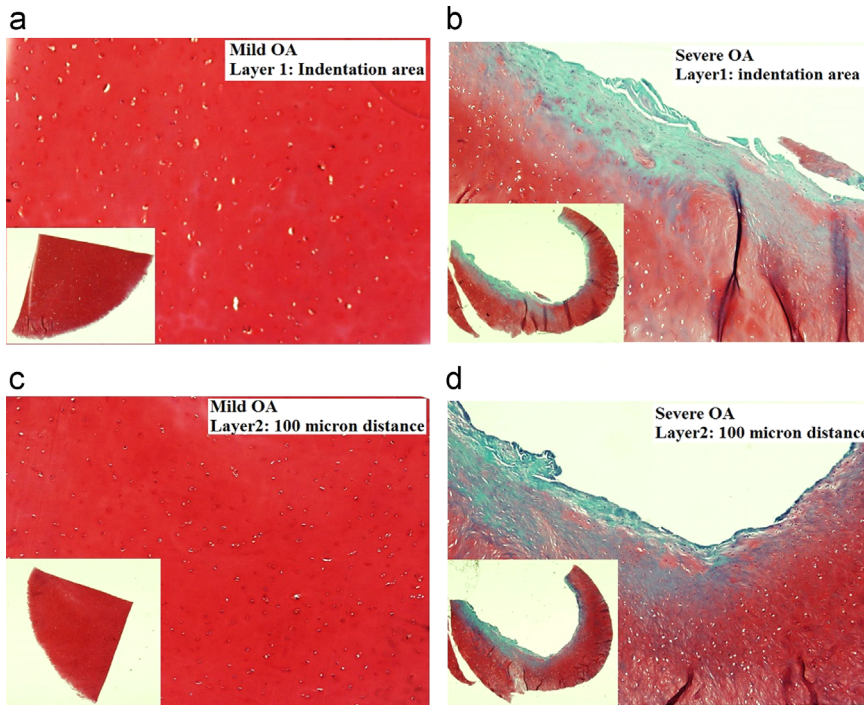


**Fig. 7 – Histology of cartilage specimens stained by Safranin-O at two different intervals. mild OA at the same area with microindentation experiment (a), severe OA at the same area with microindentation experiment (b), mild OA at 100  $\mu\text{m}$  distance from the first layer (c), severe OA at 100  $\mu\text{m}$  distance from the first layer (d).**

scan time. Next, according to the previous studies (Kok et al., 2013; Palmer et al., 2006; Xie et al., 2010), a contrast agent solution was prepared by mixing 40% Hexabrix "ioxaglate" (GE Healthcare, The Netherlands, 320 mgI/ml, MW=1269 g/mol, Charge -1), 60% PBS, pH=7.4 with protease inhibitor, which resulted in an overall osmolality of 470 mOsmol/kg.

Each sample was kept in the contrast agent medium overnight to become completely saturated with Hexabrix. Thereafter, the samples were thoroughly removed from the contrast agent medium. Pre-processing of the reconstructed images, including noise reduction, contrast adjustment, image calibration (between blank space and plastic bore in each image) and conversion to TIFF file format, was conducted using the companion software of the micro-CT machine (Analyze 11.0, USA). The mid-sagittal slice of each image from the stacks underwent global segmentation to create a binary mask corresponding to the geometry of the cartilage (imageJ, 1.47e). Afterwards, the outline of the segmented cartilage masks was placed on the cartilage image to calculate the average gray value of the area representing the cartilage. The average gray values were calculated using imageJ according to the following formulae:

$$\text{Average gray value} = \frac{\sum P_i x_i}{\sum x_i} \quad (9)$$

where and  $x_i$  are pixel intensity and pixel frequency, respectively.

#### 2.4. Histological examination

For histological evaluation, samples were fixed in 4% formaldehyde for 24 h. Afterwards, the specimens were dehydrated

in a graded ethanol series and xylene and embedded in paraffin. 5  $\mu\text{m}$  thick sections at the surface layer and at 100  $\mu\text{m}$  interval were obtained using a microtome (MICROM, Germany). Knee joint slides were examined by Safranin-O with a fast green. The stained slides were visualized using a light microscope (Olympus BX51, Japan) and images were captured by a digital camera using cellwidehatF software.

#### 2.5. Statistical analysis

The unpaired Student's t-test was used to compare the mechanical properties measured at different time points, disease severity, and tonicity. A significance threshold of 0.05 was adopted.

### 3. Results

#### 3.1. Indentation experiments

##### 3.1.1. Micro-scale

As expected Young's modulus of the cartilage decreased after immersion in the hypertonic solution. Although this is clear for 20 and 120 min immersion data, the intermediate time scales (40 and 60 min) are not clearly decreased for all the samples. After 20 min immersion in the hypertonic solution, the semi-equilibrium modulus ( $E$  in Eq. (6) decreased in 10 out of 11 locations of the indentation tests for the 5 samples (Fig. 3a,  $p=0.008$ ). Similarly, the semi-equilibrium modulus of the specimens after 120 min of immersion in the hypertonic solution was significantly less than that of the starting point ( $p=0.017$ ) (Fig. 3d). The semi-equilibrium moduli measured

after 40 and 60 min of immersion in the hypertonic solutions were not lower, but in general increased with respect to the 20 and 120 min data, indicating that after a first loss of water content (20 min) they attract water (40–60 min) and loose water again at 120 min (Fig. 3b,c). Apparently samples have their own dynamics concerning the time sequence of elasticity change (Fig. 4). Table 1 depicts the average semi-equilibrium modulus obtained by nano-indenter in microscale.

### 3.1.2. Nano-scale

Finite Gaussian mixture models with four components were found to satisfactorily capture all the peaks present in the probability density function for all levels of disease severity and medium tonicity (Fig. 5). Among the four components, the three first components consistently exhibited large weighting factors (Table 2) while the weighting factor of the last components was often (three out of four cases) very small as compared to the others (Table 2). The mean elastic modulus of the first component of the severe OA specimens was up to two times larger than the corresponding mean of the mild OA specimens (Table 2). The reverse held for the mean modulus value of the second component (Table 2). The mean values of the first two modulus peaks of the mild specimens were respectively 17% and 14% higher in the hypertonic solution as compared to the isotonic solution (Table 2). As for the third and fourth peaks, they were respectively 37% and 46% lower in the hypertonic solution. Considering the severe OA samples, the mean values of four peaks were respectively 19%, 9%, 6%, and 34% lower in the hypertonic solution as compared to the isotonic solution (Table 2).

**Table 1 – Semi-equilibrium modulus at micro-scale.**

Time points	E (MPa)	SD
Isotonic	9.88	6.08
Hypertonic (20 min)	7.00	4.40
Hypertonic (40 min)	8.89	4.75
Hypertonic (60 min)	7.42	2.75
Hypertonic (120 min)	5.23	2.67

E: average micro-stiffness; SD: standard deviation.

### 3.2. EPIC- $\mu$ CT

The average of the mean gray values calculated for the severe OA group was  $335 \pm 57$  (mean  $\pm$  SD) which was significantly higher ( $p=0.03$ ) than that of the mild OA group, i.e.  $252 \pm 19$ , indicating presence of considerably higher GAG content in the mild OA specimens as compared to the severe OA specimens. Representative specimens with an average gray value close to the mean of each group were selected for further analysis (Fig. 6b).

### 3.3. Histology

In the histopathological observation of the safranin-O slides, the mild OA samples depict nicely distributed high concentration of GAGs corresponding to the indentation experiment area. In comparison with the mild OA samples, the severe OA samples show less GAGs content as well as noticeable surface fibrillation and irregularity (Fig. 7a,b). The same pattern was found in 100  $\mu$ m interval (Fig. 7c,d).

## 4. Discussion

As the overall stiffness of cartilage highly depends on the water influx and the subsequent pre-stress of the collagen fibers both micro- and nano-mechanical behaviors of the cartilage in our experiments strongly depend on the tonicity. For the severe OA samples, the tonicity dependence was changed, likely as a result of the altered (lower) GAG content. There are, however, certain distinct patterns observed at both scales of measurement that are discussed in the following sections.

### 4.1. Micro-mechanics of OA cartilage

In micro-scale, mild OA specimens demonstrated a significant decrease in the semi-equilibrium modulus due to osmotic effects. (Boumans, 2005; Eisenberg and Grodzinsky, 1985; Selvadurai, 1996). This pattern was clear after 20 min of incubation with hypertonic PBS, as the modulus was reduced in 10 out of 11 measurement locations and significantly less elastic modulus of cartilage was observed as compared to the starting point. The same significant decrease was observed after 120 min. However, there was significant variability between samples after 40 min and 60 min that probably

**Table 2 – Maximum likelihood estimates of the parameters of the Gaussian finite mixture models when 4 Gaussian components were used.**

Sample name	$\mu_1$ (kPa)	$\mu_2$ (kPa)	$\mu_3$ (kPa)	$\mu_4$ (kPa)	$\sigma_1$ (kPa)	$\sigma_2$ (kPa)	$\sigma_3$ (kPa)	$\sigma_4$ (kPa)	$w_1$	$w_2$	$w_3$	$w_4$
mOA_N	78	248	793	2107	36	98	317	772	0.37	0.34	0.21	0.08
mOA_H	91	282	499	1143	33	99	160	185	0.39	0.30	0.23	0.08
sOA_N	177	190	442	739	67	66	87	300	0.30	0.25	0.24	0.21
sOA_H	143	174	473	553	56	1056	167	21	0.57	0.002	0.37	0.06

Mild OA in normal PBS solution: mOA\_N.

Mild OA in hypertonic PBS solution: mOA\_H.

Severe OA in normal PBS solution: sOA\_N.

Severe OA in hypertonic PBS solution: sOA\_H.

$\mu_i$ : mean;  $\sigma_i$ : standard deviation;  $w_i$ : weighting factor of every constituent.

reflect the existence of a transition state before reaching the final equilibrium state (Fig. 3b,c). One explanation might be that there are two transport time-scales that are involved, one is the movement of the water into the tissue, and the other one is the diffusion of the macromolecular osmolytes such as PGs degradation products or intact molecules freed from the swollen collagen matrix out of the tissue (Houard et al., 2013; Vynios, 2014). Transient response to osmotic loading has been also reported in computational studies of swelling and volumetric changes of multi-phasic materials under osmotic loading (Albro et al., 2007). Since the swelling behavior is driven by GAG content, these specimens may exhibit different (e.g. shifted or scaled) curves of swelling transition in response to the same osmotic loading. This could explain intra-specimen variations in the intermediate time points, i.e. 40 and 60 min after incubation in the hypertonic solution. Furthermore, Fig. 4 confirmed that each sample has its own dynamics in osmotic change response. It is also important to realize that these mild OA cartilage specimens are from different patients that may be at different stages of the diseases and, hence, have different levels of GAG content. EPIC- $\mu$ CT also shows large variations in the spatial distribution of GAGs that confirm the obvious indentation location dependency due to this topographic variation as an intrinsic feature of the cartilage tissue (Sim et al., 2015). There could therefore be large inter-specimen variations in terms of transient swelling response to changes in the tonicity that could also explain the variations observed in the intermediate time points (Siebelt et al., 2011a). It could be observed from Fig. 6 that mild and severe OA specimens were visually different in size and thickness.

#### 4.2. Nano-mechanics of OA cartilage

Only a few studies are available where the histogram or probability density function of the nano-scale elastic modulus of cartilage has been presented based on a large number (i.e. thousands) of measurements (Loparic et al., 2010). Even less data is available regarding the histogram of OA cartilage. The large number of measurements enables us to separate the mechanical behavior of the different constituents of cartilage from each other. The response of the different constituents of cartilage to certain stimuli such as changes in the osmolality of the surrounding medium could then be studied. In a study (Loparic et al., 2010) where a similar histogram of healthy cartilage was plotted based on a large number of data points, two very clear peaks were observed that the authors associated with the nano-scale elastic modulus of GAGs (22.3 kPa) and collagen (384 kPa). The results of the current study for OA cartilage show several differences with those previously reported results. First, at least four components are needed to describe the histogram (or the probability density function) of the nano-scale elastic modulus obtained in the current study. The weighting factor of one of these components is always very small. However, one needs to assume the presence of at least three Gaussian components in the finite mixture model in order to satisfactorily explain the observed distribution of peaks (Loparic et al., 2010). OA cartilage may have additional constituent with distinct mechanical properties, because some parts of

the cartilage network and/or GAG species may have been cleaved and broken down to remnant products or make changes in polymer conformation.

Comparing the mean elastic moduli observed here (Table 2, Fig. 5) with those observed previously (Loparic et al., 2010), the peaks that seem to represent the mechanical properties of GAGs and collagen network are respectively the first and third peaks. The mean elastic modulus of the third Gaussian component ( $\mu_3$ ) is much higher for mild OA specimens (793 kPa for the isotonic solution, Table 2, Fig. 5a) as compared to severe OA specimens (442 kPa for the isotonic solution, Table 2, Fig. 5c). This is consistent with the expectation that the elastic modulus of the collagen network should be higher in the mild OA specimens as compared to the severe OA specimen with its (likely) disrupted collagen network. Furthermore, assigning the third Gaussian component to the collagen network is consistent with the observation regarding the effect of tonicity on the elastic modulus of the collagen network. When tonicity increases, one expects the elastic modulus of the collagen network to decrease due to the outgoing water and decreased swelling pre-tension (dehydration effect). Consistent with this prediction, the mean elastic modulus of the third Gaussian component ( $\mu_3$ ) drastically drops from 793 kPa to 499 kPa, as the tonicity increases from isotonic to hypertonic conditions (Table 2, Fig. 5a,b). No such drop is observed for the first or second Gaussian components of the mild OA specimens, indicating that those two components are not likely to be associated with the collagen network. These observations are in agreement with Parsons and Black's study in which they discovered the lower pre-stress and subsequent tissue shrinkage in hypertonic solution as well as locally increase in PGs concentration due to resulting water redistribution (Parsons and Black, 1979). Also, lower modulus was found for bovine cartilage in response to higher concentration mediums (up to 1 M NaCl) measured using macroscale confined compression by Eisenberg and Grodzinsky (1985).

If we assume that the third Gaussian component, indeed, represents the mechanical properties of the collagen network, it is interesting to see that the severe OA specimens do not respond to changes in tonicity in the same way that mild OA specimens do. The elastic modulus of healthy or lightly disturbed cartilage (as in mild OA specimens) is higher in isotonic conditions as compared to hypertonic conditions because there is a large volume of GAG molecules in cartilage that attract water molecules, cause swelling, and create pre-stress in the collagen network. In the case of severe OA specimens, EPIC- $\mu$ CT results clearly show that there is significantly less GAG content as compared to mild OA since there is an inverse relationship with GAGs distribution and negatively charged contrast agent (Bansal et al., 2010; Piscaer et al., 2008; Siebelt et al., 2011b; Xie et al., 2010). The mild OA samples demonstrates lower x-ray attenuation of ioxaglate equivalent to higher GAG content compared to severe OA samples with higher x-ray attenuation of ioxaglate equivalent to low GAG content (Fig. 6b). Moreover, the collagen network is already damaged in the severe OA as compared to mild OA specimens, as is clear from much lower elastic modulus of the collagen network of severe OA specimens in the isotonic solution (442 kPa, Fig. 5c) as compared to the

elastic modulus of the collagen network of mild OA specimens (793 kPa, Fig. 5a). One could therefore conclude that presence of GAG molecules and a strong collagen network that could be put under pre-stress are lacking in severe OA specimens and that is why severe OA specimens do not respond to tonicity changes. Since most of AFM-based studies have considered two regions over the cartilage stiffness histogram obtained from force displacement curves, we compared the histograms between two- and four-component Gaussian distributions. The data from two-component Gaussian distribution presents the same trends as the four-component distribution for all conditions considered here.

The above-mentioned mechanisms are some of the physical mechanisms that govern the nano-scale mechanical behavior of cartilage. In addition to those factors, it should be also noted that the nano-scale elastic modulus of cartilage depends on the ionic and non-ionic portions of the cartilage tissue (Rauker et al., 2014). In other words, GAG chains with their negative charge can interact with positive ions from the environment and distinguish themselves in certain ways, i.e. crosslinking density of the long chains, molecular weight number between crosslinking portions, the tortuosity of the pores, entanglement length, and filament bundle diameter (Miriam et al., 2010; Moeendarbary et al., 2013). Moreover, these changes are also detectable in the GAG fragments that are noticeably present in the OA cartilage. These are some of the influential factors in the modulus of the polymeric molecules. For instance, the modulus is directly related to the crosslinking density of the polymeric chains and network. By increasing positive ion concentrations, the probability of interactions and entanglements for both GAG macromolecules and fragments rises and therefore a higher modulus will be predicted than what was observed for the first and second peaks of mild samples (78 and 91 kPa see Fig. 5a,b) in isotonic solution compared to (248 and 282 kPa, see Fig. 5a,b) in hypertonic solution. On the other hand, collagen fibers do not contain the ionic part on their chains and the reduction in the stiffness of the collagenic molecules demonstrates the effects of swelling pressure and less amount of pre-stress, as previously discussed (Moeendarbary et al., 2013; Parsons and Black, 1979; Selvadurai, 1996).

In a general sense, indentation experiments are neglecting the possibility of some intrinsic interactions between the tip and surface of the sample specifically in nano-scale. The examples include intramolecular interactions, adhesion, and electrostatic forces (Drira and Yadavalli, 2013; Moshtagh et al., 2014; Rauker et al., 2014). Some other limitations arise from the nanoindentation techniques themselves. For example, one needs to apply specific theoretical assumptions – specifically about the size and shape of the tips - to be able to calculate the modulus. These may cause certain levels of inaccuracies in nanoindentation measurements in general. The effects of the above-mentioned limitations of the nanoindentation techniques on the obtained results have been extensively discussed in the literature (Rauker et al., 2014). In addition, it should be noted that nanoindentation measurements probe the mechanical properties of cartilage (components) at the surface, which do not necessarily represent those found in the bulk of the tissue. Nevertheless, the

surface properties are found to be good indicators of OA onset and progression (Desrochers et al., 2012; Guilak et al., 1994; Panula et al., 1998).

## 5. Conclusion

In summary, the results of this study show that the micro- and nano-scale mechanical behavior of OA cartilage is dependent on the tonicity of the surrounding medium and may change as the disease progresses from its initial stages to the more severe stages. The micro-scale elastic modulus of mild OA cartilage decreases in the hypertonic solution as compared to the isotonic solution. Moreover, each sample has its own specific dynamic behavior response to tonicity. EPIC- $\mu$ CT also shows the dependency of the indentation assay to the test location. In the nano-scale, the histogram of the elastic modulus of both mild and OA cartilage specimens and the associated finite mixture analysis show the presence of three to four distinct constituents with their own distinct peaks. Comparing the mean elastic moduli of the first three peaks with those of previous studies indicates that the first and third peaks are respectively associated with GAGs and collagen network. In mild OA specimens, the mean elastic modulus of the peak associated with the collagen network is lower in the hypertonic solution as compared to the isotonic solution. Moreover, the mean value of the peak associated with collagen network is higher in mild OA specimens as compared to severe OA specimens (both in isotonic solutions). Both above-mentioned observations support the assumption that the third Gaussian components represent the nano-scale mechanical properties of the collagen network. There is no direct evidence in the current study to support the assumption that the first mixture component represents the nano-scale mechanical properties of GAGs. For severe OA specimens, neither the peak associated with the collagen network nor the one associated with GAGs show any decrease when the tonicity changes. These observations suggest that the sensitivity of the nano-scale mechanical properties of OA specimens to tonicity may vanish as GAGs lose.

## Acknowledgments

We gratefully acknowledge the Dutch Arthritis Foundation (Reumafonds, 13-3-406) for its financial support.

## REFERENCES

- Albro, M.B., Chahine, N.O., Caligaris, M., Wei, V.I., Likhitpanichkul, M., Ng, K.W., Hung, C.T., Ateshian, G.A., 2007. Osmotic loading of spherical gels: a biomimetic study of hindered transport in the cell protoplasm. *J. Biomech. Eng.* 129, 503–510.
- Athanasiou, K.A., Rosenwasser, M.P., Buckwalter, J.A., Malinin, T. I., Mow, V.C., 1991. Interspecies comparisons of *in situ* intrinsic mechanical properties of distal femoral cartilage. *J. Orthop. Res.* 9, 330–340.
- Bansal, P.N., Joshi, N.S., Entezari, V., Grinstaff, M.W., Snyder, B.D., 2010. Contrast enhanced computed tomography can predict

- the glycosaminoglycan content and biomechanical properties of articular cartilage. *Osteoarthr. Cartil.* 18, 184–191.
- Boumans, J.H.W., 2005. Swelling and Curling Behaviors of Articular Cartilage from Bovine Knee Joints. Columbia University New York and Technical University Eindhoven.
- Desrochers, J., Amrein, M.W., Matyas, J.R., 2012. Viscoelasticity of the articular cartilage surface in early osteoarthritis. *Osteoarthr. Cartil.* 20, 413–421.
- Drira, Z., Yadavalli, V.K., 2013. Nanomechanical measurements of polyethylene glycol hydrogels using atomic force microscopy. *J. Mech. Behav. Biomed. Mater.* 18, 20–28.
- Eisenberg, S.R., Grodzinsky, A.J., 1985. Swelling of articular cartilage and other connective tissues: electromechanochemical forces. *J. Orthop. Res.* 3, 148–159.
- Ghosh, P., Smith, M., 2002. Osteoarthritis, genetic and molecular mechanisms. *Biogerontology* 3, 85–88.
- Guilak, F., Ratcliffe, A., Lane, N., Rosenwasser, M.P., Mow, V.C., 1994. Mechanical and biochemical changes in the superficial zone of articular cartilage in canine experimental osteoarthritis. *J. Orthop. Res.* 12, 474–484.
- Han, L., Frank, E.H., Greene, J.J., Lee, H.Y., Hung, H.H., Grodzinsky, A.J., Ortiz, C., 2011. Time-dependent nanomechanics of cartilage. *Biophys. J.* 100, 1846–1854.
- Hedbom, E., Hauselmann, H.J., 2002. Molecular aspects of pathogenesis in osteoarthritis: the role of inflammation. *Cell. Mol. Life Sci.* 59, 45–53.
- Houard, X., Goldring, M.B., Berenbaum, F., 2013. Homeostatic mechanisms in articular cartilage and role of inflammation in osteoarthritis. *Curr. Rheumatol. Rep.* 15, 375.
- Ishiguro, N., Poole, A.R., Kojima, T., 2002. Mechanism of cartilage destruction in osteoarthritis. *Nagoya J. Med. Sci.* 65, 73–84.
- Jin, H., Lewis, J.L., 2004. Determination of Poisson's ratio of articular cartilage by indentation using different-sized indenters. *J. Biomech. Eng.* 126, 138–145.
- Julkunen, P., 2008. Relationships between structure composition and function of articular cartilage. *Nat. Environ. Sci.* 235 (Kuopio University).
- Kok, A.C., Tuijthof, G.J., den Dunnen, S., van Tiel, J., Siebelt, M., Everts, V., van Dijk, C.N., Kerkhoffs, G.M., 2013. No effect of hole geometry in microfracture for talar osteochondral defects. *Clin. Orthop. Relat. Res.* 471, 3653–3662.
- Li, C., Allen, J., Alliston, T., Pruitt, L.A., 2011. The use of polyacrylamide gels for mechanical calibration of cartilage – a combined nanoindentation and unconfined compression study. *J. Mech. Behav. Biomed. Mater.* 4, 1540–1547.
- Loparic, M., Wirz, D., Daniels, A.U., Raiteri, R., Vanlandingham, M.R., Guex, G., Martin, I., Aebi, U., Stoltz, M., 2010. Micro- and nanomechanical analysis of articular cartilage by indentation-type atomic force microscopy: validation with a gel-microfiber composite. *Biophys. J.* 98, 2731–2740.
- Miller, G.J., Morgan, E.F., 2010. Use of microindentation to characterize the mechanical properties of articular cartilage: comparison of biphasic material properties across length scales. *Osteoarthr. Cartil.* 18, 1051–1057.
- Miriam, V., Flores-Merino, S.C., Caterina, LoPrestia, Gwendolen C., Reilly, Giuseppe, Battaglia, Adam, J. Engler, 2010. Nanoscopic mechanical anisotropy in hydrogel surfaces. *Soft Matter* 6 (18), 4466–4470.
- Moeendarbarry, E., Valon, L., Fritzsche, M., Harris, A.R., Moulding, D.A., Thrasher, A.J., Stride, E., Mahadevan, L., Charras, G.T., 2013. The cytoplasm of living cells behaves as a poroelastic material. *Nat. Mater.* 12, 253–261.
- Moshtagh, P.R., Rauker, J., Sandker, M.J., Zuiddam, M.R., Dirne, F.W., Klijnstra, E., Duque, L., Steendam, R., Weinans, H., Zadpoor, A.A., 2014. Nanomechanical properties of multi-block copolymer microspheres for drug delivery applications. *J. Mech. Behav. Biomed. Mater.* 34, 313–319.
- Moyer, J.T., Abraham, A.C., Haut Donahue, T.L., 2012. Nanoindentation of human meniscal surfaces. *J. Biomech.* 45, 2230–2235.
- Nia, H.T., Han, L., Li, Y., Ortiz, C., Grodzinsky, A., 2011. Porelasticity of cartilage at the nanoscale. *Biophys. J.* 101, 2304–2313.
- Nia, H.T., Bozchalooi, I.S., Li, Y., Han, L., Hung, H.H., Frank, E., Youcef-Toumi, K., Ortiz, C., Grodzinsky, A., 2013. High-bandwidth AFM-based rheology reveals that cartilage is most sensitive to high loading rates at early stages of impairment. *Biophys. J.* 104, 1529–1537.
- Nimer, E., Schneiderman, R., Maroudas, A., 2003. Diffusion and partition of solutes in cartilage under static load. *Biophys. Chem.* 106, 125–146.
- Oyen, M.L., 2013. Nanoindentation of biological and biomimetic materials. *Exp. Tech.* 37, 73–87.
- Oyen, M.L., Cook, R.F., 2009. A practical guide for analysis of nanoindentation data. *J. Mech. Behav. Biomed. Mater.* 2, 396–407.
- Palmer, A.W., Guldberg, R.E., Levenston, M.E., 2006. Analysis of cartilage matrix fixed charge density and three-dimensional morphology via contrast-enhanced microcomputed tomography. *Proc. Natl. Acad. Sci.* 103, 19255–19260.
- Panula, H.E., Hyttinen, M.M., Arokoski, J.P., Langsjo, T.K., Pelttari, A., Kiviranta, I., Helminen, H.J., 1998. Articular cartilage superficial zone collagen birefringence reduced and cartilage thickness increased before surface fibrillation in experimental osteoarthritis. *Ann. Rheum. Dis.* 57, 237–245.
- Parsons, J.R., Black, J., 1979. Mechanical behavior of articular cartilage: quantitative changes with alteration of ionic environment. *J. Biomech.* 12, 765–773.
- Piscaer, T.M., Waarsing, J.H., Kops, N., Pavljasevic, P., Verhaar, J.A., van Osch, G.J., Weinans, H., 2008. In vivo imaging of cartilage degeneration using microCT-arthrography. *Osteoarthr. Cartil.* 16, 1011–1017.
- Rauker, J., Moshtagh, P.R., Weinans, H., Zadpoor, A.A., 2014. Analytical relationships for nanoindentation-based estimation of mechanical properties of biomaterials. *J. Mech. Med. Biol.* 14, 14300041–14300044.
- Richard, F., Villars, M., Thibaud, S., 2013. Viscoelastic modeling and quantitative experimental characterization of normal and osteoarthritic human articular cartilage using indentation. *J. Mech. Behav. Biomed. Mater.* 24, 41–52.
- Selvadurai, A.P.S., 1996. Mechanics of Poroelastic Media Springer Science+Business Media Dordrecht. McGill University, Montreal, Quebec, Canada.
- Siebelt, M., Waarsing, J.H., Kops, N., Piscaer, T.M., Verhaar, J.A., Oei, E.H., Weinans, H., 2011b. Quantifying osteoarthritic cartilage changes accurately using in vivo microCT arthrography in three etiologically distinct rat models. *J. Orthop. Res.* 29, 1788–1794.
- Siebelt, M., van Tiel, J., Waarsing, J., Piscaer, T., van Straten, M., Booij, R., Dijkshoorn, M., Kleinrensink, G.J., Verhaar, J., Krestin, G., Weinans, H., Oei, E.H., 2011a. Clinically applied CT arthrography to measure the sulphated glycosaminoglycan content of cartilage. *Osteoarthr. Cartil.* 19, 1183–1189.
- Sim, S., Hadjab, I., Garon, M., Quenneville, E., Buschmann, M.D., 2015. Relevance of the spatial distribution pattern of mechanical properties of articular cartilage in animal studies. In: Proceedings of the Annual Meeting Orthopedic Research Society.
- Stoltz, M., Raier, R., Daniels, A.U., VanLandingham, M.R., Baschong, W., Aebi, U., 2004. Dynamic elastic modulus of porcine articular cartilage determined at two different levels of tissue organization by indentation-type atomic force

- microscopy. *Biophys. J.* 86, 3269–3283.
- Stolz, M., Gottardi, R., Raiteri, R., Miot, S., Martin, I., Imer, R., Stauffer, U., Raducanu, A., Duggelin, M., Baschong, W., Daniels, A.U., Friederich, N.F., Aszodi, A., Aebi, U., 2009. Early detection of aging cartilage and osteoarthritis in mice and patient samples using atomic force microscopy. *Nat. Nanotechnol.* 4, 186–192.
- Vynios, D.H., 2014. Metabolism of cartilage proteoglycans in health and disease. *Biomed. Res. Int.* 2014, 452315.
- Wilusz, R.E., Zauscher, S., Guilak, F., 2013. Micromechanical mapping of early osteoarthritic changes in the pericellular matrix of human articular cartilage. *Osteoarthr. Cartil.* 21, 1895–1903.
- Xie, L., Lin, A.S.P., Guldberg, R.E., Levenston, M.E., 2010. Nondestructive assessment of sGAG content and distribution in normal and degraded rat articular cartilage via EPIC- $\mu$ CT. *Osteoarthr. Cartil.* 18, 65–72.
- Zadpoor, A.A., 2015. Nanomechanical characterization of heterogeneous and hierarchical biomaterials and tissues using nanoindentation: the role of finite mixture models. *Mater. Sci. Eng. C* 48, 150–157.